A NEW GLOBAL SCALE RIVER'S SLOPE DATASET

by

TONG WAN

SAGY COHEN, COMMITTEE CHAIR

LISA DAVIS
YONG ZHANG

A THESIS

Submitted in partial fulfillment of the requirements
for the degree of Master of Science
in the Department of Geography
in the Graduate School of
The University of Alabama

TUSCALOOSA, ALABAMA

2016

ABSTRACT

River's slope (bed and flow) is a key parameter in fluvial hydrology, hydraulics and geomorphology. It affects many important fluvial variables such as flow velocity and sediment transport, especially bedload. Limitation in river's slope data confined fluvial modeling, particularly at large scales. Traditional slope calculation algorithms cannot accurately predict river's slopes as these are based on cell-by-cell calculation, which is only suitable for hillslopes and steep mountainous streams. This paper presents a new algorithm for calculating global river's slope and a procedure to upscale it for relatively course resolution global hydrological modeling. The algorithm is based on a simple principle of calculating slope from elevation depression over the length of a river segment. The algorithm automates this calculation for global rivers. In this paper, the HydroSHEDS 15 arc-sec Digital Elevation Model is used for calculating global river network and retrieving the elevation values. A sensitivity analysis is conducted in order to examine the effect of maximum river segment length on slope predictions. An analysis of the accuracy of this dataset has been conducted by comparing the new dataset against observed slope data collected from the literature and an independent high-resolution stream network layer for the contiguous United States. The results show that this algorithm is able to accurately calculate global river's slope. Applications of the resulting dataset are proposed.

LIST OF ABBREVIATIONS AND SYMBOLS

V	cross-sectional average velocity
k	unit conversion factor
n	Manning's coefficient
R	hydraulic radius
S	slope
GIS	Geographic Information System
DEM	Digital Elevation Model
NHD	National Hydrography Dataset
HydroSHEDS	Hydro SHuttle Elevation Derivatives
NED	National Elevation Dataset
WBD	Watershed Boundary Dataset
RMSE	Root Mean Square Error
R2	coefficient of determination
Fig.	Figure
WBMsed	Water Balance Model (sediment)
Qb	daily bedload flux
Qi	daily mean water discharge
ρ_s	sediment density
ρ	fluid density

e_b	bedload efficiency
λ	limiting angle of repose of sediment grains lying on the river bed
=	Equal to
>	Greater than
<	Less than

ACKNOWLEDGMENTS

There are scads of people without whom this thesis might not have been written, and to whom I am indebted.

To Dr. Sagy Cohen, the chairman of this thesis and also my supervisor for the whole research, who has taken me to the world of science and guided me to finish the whole thesis research. I am always full of courage while working with him because he encouraged me when I was down and inspired me when I was lost. This research cannot be finished without many python scripts he wrote before and this thesis cannot be written without his help on English writing.

To my committee members, Dr. Lisa Davis and Dr. Yong Zhang, thanks for being my committee member and having my thesis proposal approved. Your comments and suggestions on my proposal helped me a lot on my thesis research and promote my thesis writing.

To Shawn Carter and Monica Stone, my dear lab colleagues and life-time friends, who helped me to become adapted to a brand new life in U.S. and taught me everything I do not know before and never get tired. The most unforgettable time I had during these two years are moments we spent together in our lab.

To my dear family, who supported me all the time and made me feel the warmth of family and motivated me to persist even though they are thousands of miles away.

CONTENTS

LIST OF TABLES

LIST OF FIGURES

CHAPTER 1

INTRODUCTION

River's slope is a key parameter in many fluvial processes; including flow velocity, sediment transport and river morphology. It not only describes the steepness of rivers, but also offers signal of river dynamics as rivers tend to adjust the slope with both external (e.g. tectonic uplift, climate change) and internal (e.g. water discharge, river width) changes.

As a factor related to river's slope, flow velocity has a major impact on fluvial processes and river dynamics. It is responsible for many of the physical characteristics of a stream and is a crucial factor for simulating flow dynamics in hydrological models (Hagemann and Dumenil, 1997). Velocity is also a dominant control on fluvial transport capacity of sediment and other particulates. River's flow velocity is also influenced by other river parameters including: width and depth of the stream and the roughness of the substrate or stream bottom. Among different flow velocity models, the Manning-Strickler formula has been frequently applied to simulate fluvial flow velocity (e.g. Arora and Boer, 1999; Schulze et al., 2005; NgoDuc et al., 2007) and was demonstrated as enhancing the representations of flow velocities (Schulze et al., 2005). In Manning's equation (Manning, 1891), flow velocity is driven by gravity and determined by hydraulic radius, slope and Manning's coefficient and states as:

$$V = \frac{k}{n} R_h^{2/3} S^{1/2} \quad (1)$$

Where V is the cross-sectional average velocity (m/s); n is the Manning's coefficient, R is the hydraulic radius (m); S is the slope and k is a unit conversion factor. As Manning's equation is widely used, river slope is a necessary variable for geomorphologists to obtain.

The relationship between slope and sediment has long been known (e.g. Du Boys, 1879; Meyer-Peter et al., 1948; Bagnold, 1966). Decrease of a river slope tends to result in reduction in sediment transport potential in rivers, particularly for bedload. This control on sediment load, in addition to velocity and discharge, has a direct influence on river morphology and behavior. Change in slope is able to drive adjustment of dynamic equilibrium in an alluvial stream (Mackin et al., 1948). A number of researches also showed that regions of decreasing slopes along a river network tend to have more frequent inundation from flooding because of the change of potential erosive and transport power (Bridge, 2003). This morphological process response of streams to slope change makes slope more important in flow regime and more valuable to be quantified.

One main driver on slope change can be bed material. It is possible for a difference in bedrock resistance to cause a change in slope, especially for ungraded rivers (Carlston, 1969). Slope was shown to have short-term (up to decades) response to river sinuosity and braiding. Slope increases while river sinuosity increases and decreases when river sinuosity decreases (Schumm, 1986; Holbrook and Schumm, 1999; Schumm et al., 2000; Burbank and Anderson, 2001; Bridge, 2003). In addition to sinuosity, water discharge and sediment also have a vital effect on slope. Increase of slope sometimes forms as a result of seismic events, which brings in a problem of increased gradient shedding and increased sediment flux (Bridge, 2003). Slope change with discharge is an important fluvial mechanism. Accommodation of water on one hand forms the channel, and the remaining constant necessitates an increase in slope (Bridge, 2003).

In conclusion, slope is dependent on different variables and it has been demonstrated, from long-term monitoring of the evolution of rivers, that adjustments in these parameters can be co-dependent (Mackin et al., 1948.). Furthermore, the dynamics between slope and other fluvial parameters can considerably vary under different settings and conditions (Biedenharn et al.,

2000). These dynamics complicates spatially and temporally continues representation of slope in rivers. Many studies attempted to represent slope change using specific case studies (Gregory and Schumm, 1987; Snow and Slingerland, 1987; Knighton, 1999), all at relatively small scales.

According to the difficulty in measuring slope, some models and methods for calculating slope were developed over the years. Knighton (1998) used the local elevation change over the longitudinal profile and the channel length to calculate the slope and it can only be applied at a reach scale since elevation data need to be determined. Biedenharn et al. (2000) used this method to calculate slope for the lower Mississippi river. They calculated the slope by dividing the difference of the elevation from the maximum and minimum stage readings by the river distance between gauging stations, which was obtained from a topographic map. Most researches with different investigation goals use this method to determine the slope only at a reach scale (e.g. Montgomery and Brandon, 2002).

Traditional GIS slope calculation algorithms are based on the 'steepest-descent' approach (D8 algorithm; O'Callaghan and Mark, 1984), in which the difference in elevation between a grid cell (in a Digital Elevation Model (DEM)) and one of its eight adjacent cells, the one with the lowest elevation, is used to calculate the cell's slope. Some GIS algorithms were adjusted for calculating river slope by calculating the total distance from a cell to another downstream point or directly the cell's basin outlet. In using this method, all the cells from this certain cell to outlet cell is considered in the calculation (e.g. Moore et al., 1991; Thieken et al., 1999; Walker and Willgoose, 1999; Olivera, 2001; Fekete et al., 2001; Olivera and Raina, 2003; Reed, 2003; Mayorga et al., 2005; Lin et al., 2006). These approaches are highly inaccurate when applied to relatively coarse resolution DEMs, used in regional and global scale modeling, as cells typically include both river and surrounding landscape and cannot capture small scale meandering and

thus under represent river's length. Calculating fluvial slope using high resolution DEMs can also be problematic when the cell size is smaller than the river width. In any case the vertical accuracy of most DEMs tend to be smaller than fluvial slope in large river. For example the slope of the lower Mississippi River was estimated to be 0.00004 m/m (a drop of 1 meter over 25km), much lower than the vertical accuracy of even high resolution DEMs.

Here we introduce a new slope calculation algorithm for large rivers. Instead of using the elevation difference from one cell to an adjacent cell or the river outlet, we use the difference between maximum elevation and minimum elevation value along a river reach or river segment. The algorithm is automated within a GIS framework and is applied globally. While the reach-scale slope calculation concept behind this algorithm is simple and is not new (based on Hannon, 2011) automating it for global application and the resulting dataset is highly novel.

This paper describes the methodology and presents results of a sensitivity analysis to estimate optimal stream segment split distance and a validation procedure against observed data from the literature. Because of the limited number of observed slope data in large rivers globally, the analysis presented here also compares the results against the National Hydrography Dataset (NHDplus) dataset (Mckay et al., 2012) in U.S. rivers. A discussion of both the accuracy of the new dataset and some future applications for it are provided.

CHAPTER 2

METHODS

The new river's slope calculation methodology is based on the Hannon (2011) approach, in which slope is calculated for a given river segment based on to the difference between its highest and the lowest elevation (derived from an underlying DEM) which ideally (absent errors) corresponds to its most upstream and downstream locations respectively.

The DEM and stream-network layers used in this study are from the SHuttle Elevation Derivatives at multiple Scales (HydroSHEDS) global scale products at 15arc-sec resolution (approximately 460x460m), obtained from the USGS HydroSHEDS website (http://hydrosheds.cr.usgs.gov/index.php). The HydroSHEDS 15 arc-sec product is provided as GIS files for each continent. Corresponding flow direction and accumulated area datasets are also available for these continents in 15 arc-sec resolution. The HydroSHEDS products are limited to below latitude 60°N and so a 1arc-min resolution *etopo* DEM (Amante and Eakins, 2009.) was used for higher latitudes. Unlike HydroSHEDS, river network layers are not available for *etopo* and had to be calculated using the standard stream delineation methodology (described in section 2.1 below).

The river's slope calculation methodology (Figure 2.1) is based on the following sequence of operations:

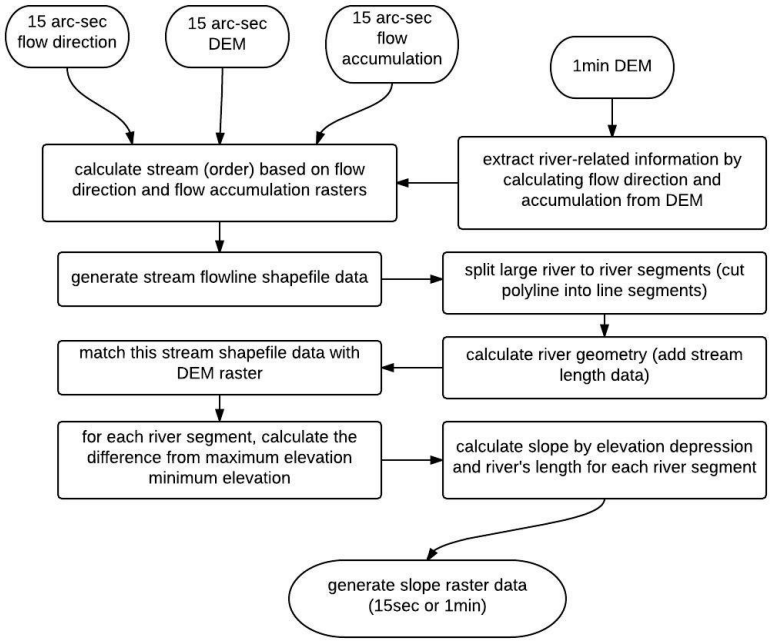

Figure 2.1 process of calculating slope based on Hannon's method

1. Obtain or delineate the stream-network (in vector format) of each continent:

This step generates the river stream-lines based on the landscape topography. Elevation change is used to calculate flow direction based on to the D8 method, which considers that water from one cell will flow towards an adjacent cell with the lowest elevation. Once the water flow direction is calculated continuously based on cell-by-cell topography, accumulated flow drainage area are calculated according to the flow direction and a completely connected flow network will be delineated. In this study, streamlines are delineated continentally. Fifteen arc-sec DEMs are used for each continent to generate the corresponding stream-network. A one arc-min etopo DEM is also used for area with a latitude higher than 60°N. The stream-network delineated from this step are vector datasets converted from the original stream raster data. Projection is also defined for these stream-networks in order to be applied in later research.

2. Split stream features to a specified maximum reach length:

In this study, streams are defined to as consisting of a number of segments based on Mackin (1948) theory that a graded stream profile comprises of a sequence of intersected segments with various slope values. Slope can vary considerably along river length and so slope should not be calculated for an entire river length or even for very long segments. Splitting rivers into smaller reaches will increase the spatial resolution of the resulting slope dataset but will also increase its sensitivity to DEM vertical and spatial biases. Here three splitting thresholds (the maximum reach length) are tested: 20, 50 and 100 km. Figure 2.3 shows the points along rivers at which rivers have been split. The distance between points is mostly even; these are reaches at the length of the splitting threshold. Some reaches are shorter following "natural" splitting points at the stream-network confluences.

An ArcGIS tool was developed to automate the splitting procedure for the entire stream-network. The tool asks the user to input the stream-network polyline layer and a value for the maximum reach length (e.g. 50 km). The tool operation starts by generating points along the stream network every e.g. 50km. Joints (splitting point) are then added to the original stream-network polyline features at the splitting points locations.

Figure 2.2 Rivers split into 50km segments

3. Extract the minimum and maximum elevation and length of each river segment:

In this study, a standard GIS tool (ArcGIS 'Zonal Statistics') is used to extract the minimum and maximum values of the DEM cells underlying each river segment. The length of each segment is also calculated using a standard GIS procedure by tracing the polyline and measuring it based on the projection unit. These are added to the stream-network layer attribute table. This procedure was automated here using a Python script.

Since water flows from high to low elevation, the start of each river segment should have the highest elevation value and the end of this segment should have the lowest elevation value among all underlying DEM cells.

4. Calculate slope for each river segment

Elevation depression, the difference between maximum and minimum elevations, is calculated for each river segment by determining the difference between maximum and minimum elevation in each river segment:

$$Elevation\ Depression\ = Maximum\ Elevation - Minimum\ Elevation$$

Slope is then calculated by:

$$slope = \frac{Elevation\ Depression}{Segment\ Length} \quad (2)$$

These calculations are done within a GIS framework and the resulting slope value for each river segment is recorded in the stream-network layer attribute table. These steps are also included in the aforementioned Python script.

5. Data conversion and upscaling

The stream-network polyline layers (one for each continent) are first converted into 15 arc-sec raster layers, corresponding to the original DEM resolution, based on the calculated slope attribute of each river segment. The continental raster layers are then mosaicked into a global-scale slope layer. An upscaling procedure was developed to reduce the raster layer resolution from 15 arc-sec to 6 arc-min (about 11x11 km) resolution to make it suitable for global-scale modeling. The standard GIS upscaling procedure calculates the average values of the fine resolution grid-cells underlying each coarse resolution grid-cell. For example, when upscaling the 15 arc-sec raster to a 6 arc-min, every grid-cell in the 6 arc-min layer has 24×24 underlying 15 arc-sec grid-cells (see illustration in Figure 2.3). Since a grid-cells in a 6 arc-min layer will, with the exception of very large rivers, cover both small and large rivers but is intended to represent the largest river in the underlying area – averaging the slope values of the fine resolution raster will over predict slope. This is because large rivers almost always have lower slopes than their tributaries. To alleviate this problem the upscaling procedure developed here extracts the minimum value of the underlying high-resolution cells and uses it as the value for the upscaled raster layer. This upscaling procedure was developed and executed using Python scripting.

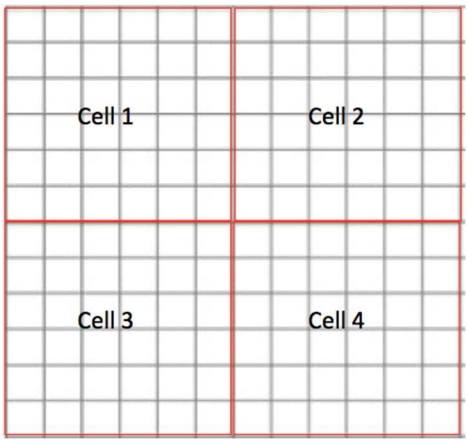

Figure 2.3 Illustration of the upscaling 'neighborhood' (1 arc-min raster into 6 arc-min raster in this case).

6. Splitting length sensitivity analysis and validation

Once slope has been calculated, a validation of the accuracy of the slope result has been conducted. Slope measurement in large rivers is difficult, and as a result, there are very few reported slope values in the literature or data repositories. Here 11 reported slope values along four large U.S. rivers (Mississippi, Arkansas, Roanoke and Ohio Rivers) were used to evaluate the accuracy of the new river's slope dataset. These slope estimates, reported in two independent studies, were derived by calculating slope from elevation depression between two gauging stations and measured river section lengths from one station to another downstream station.

The NHDplus dataset was also used as a secondary source of evaluation. NHDplus v2 is a geospatial, hydrologic framework dataset by the U.S. Environmental Protection Agency (Mckay et al., 2012). It is an incorporated set of application-ready geospatial datasets that integrate features of the National Hydrography Dataset (NHD), the National Elevation Dataset (NED) and the Watershed Boundary Dataset (WBD) based on the medium resolution NHD (1:100,000-scale). It divides the U.S. continent into 21 drainage areas and includes the stream network and elevation-derived catchments (Mckay et al., 2012). Here the stream slope attribute is used. NHDplus slope estimates were calculated in a similar way to our methodology, but using

higher resolution DEM and more detailed and better curated stream network. For validating the new slope dataset, 500 random points were generated in ArcGIS on top of the NHDplus layer. NHDplus streams with a basin area smaller than 1000 km^2 were excluded from to ensure that only rivers are compared. The slope values from the NHDplus and the new slope dataset were extracted for each point location using standard GIS procedure.

The validation analysis was coupled with a sensitivity analysis of the rivers splitting length to determine the optimal length for river segments. The results of the slope calculation procedure were evaluated for North America using a splitting threshold of 20 km, 50 km and 100 km.

CHAPTER 3

RESULTS AND DISCUSSION

The 6 arc-min resolution raster global river's slope dataset shows slope values increasing from the dark blue color to the dark red color (Figure 3.1). Most river slopes are in a dark blue color at a global scale, indicating values of 0.0001-0.0005 m/m.

As figure 3.1 shows, at the west edges of the Amazon basin (zoomed-in within the bottom-left circle), channels' slopes are high and reach values of about 0.2 m/m. High slope are also easily observable at the boundaries of several water basins. In Australia for example, high slope appears at the boundary of Murray-Darling Basin. In South Africa, high slope also shows at the boundary of Orange-Senqu Basin. At the boundary of Nile Basin, high slope occurs as well. In Europe and Asia, high slope shows at the boundary of 6 large river basins: Amur basin, Yenisei basin, Ob basin, Changjiang basin, Ganges basin and Indus Basin. At the boundary of the Yukon basin, Columbia basin, Colorado Basin and Rio Grande basin in North America, slope is as high as 0.05-0.1m/m. These high slope values are expected as river slopes are highest at a basin headwaters. This however demonstrates that the slope dataset is highly sensitive to intra-basin spatial dynamics, even at this resolution, showing that the slope values can range by over three orders of magnitudes within large river basins.

High river's slope values seem to correspond well to high water stress in many regions worldwide (Figure 3.2). High slope area in west edge of South America has a water stress index above 1, which indicates arid property. Similar patterns of high slope appear on the west edge of

North America, the east edge of Australia, and the boundaries of water basins between Europe and Asia. And generally, a high slope area is accompanied by aridity problems.

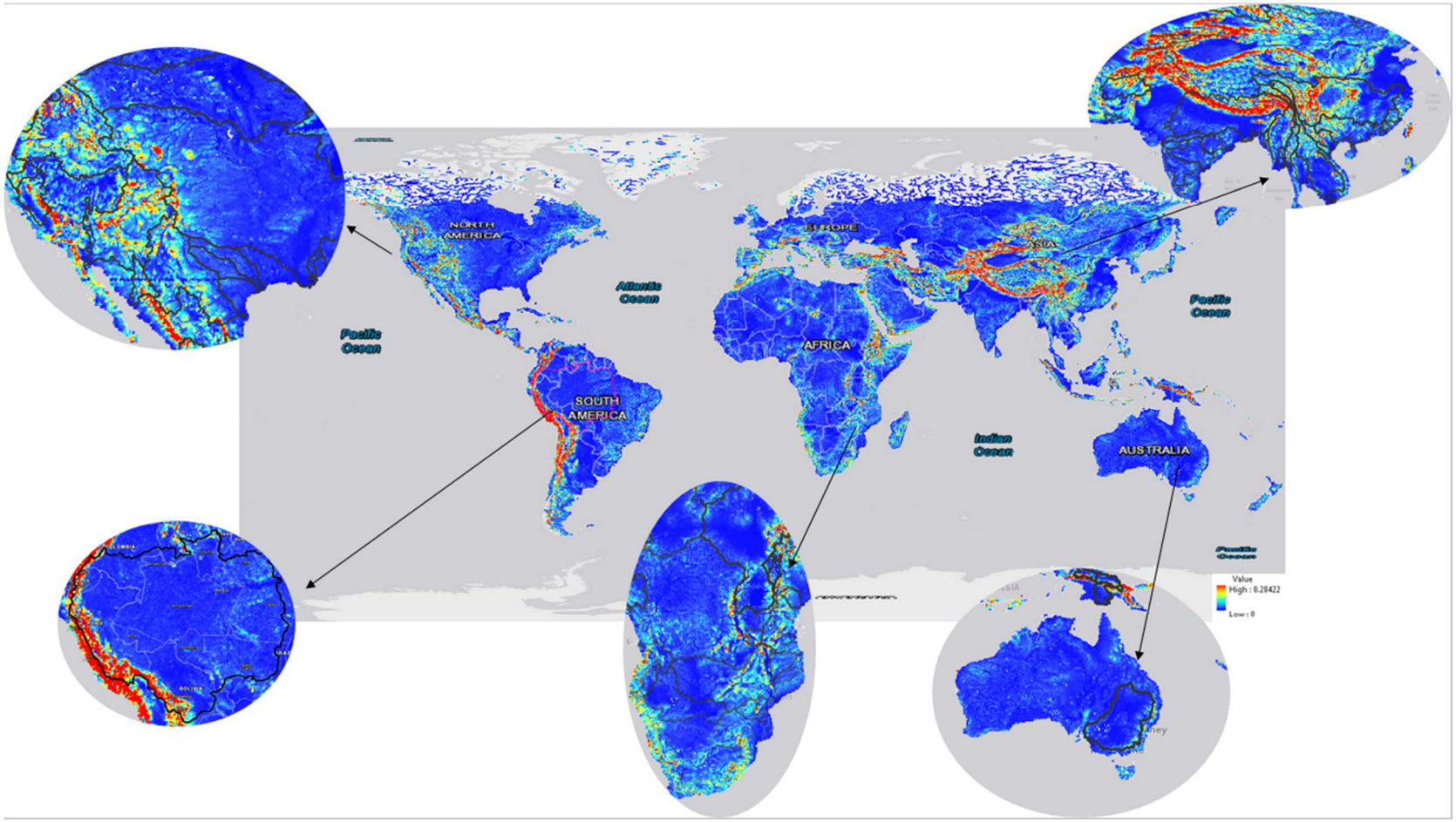

Figure 3.1 Calculated slope raster at 6 arc-min spatial resolution.

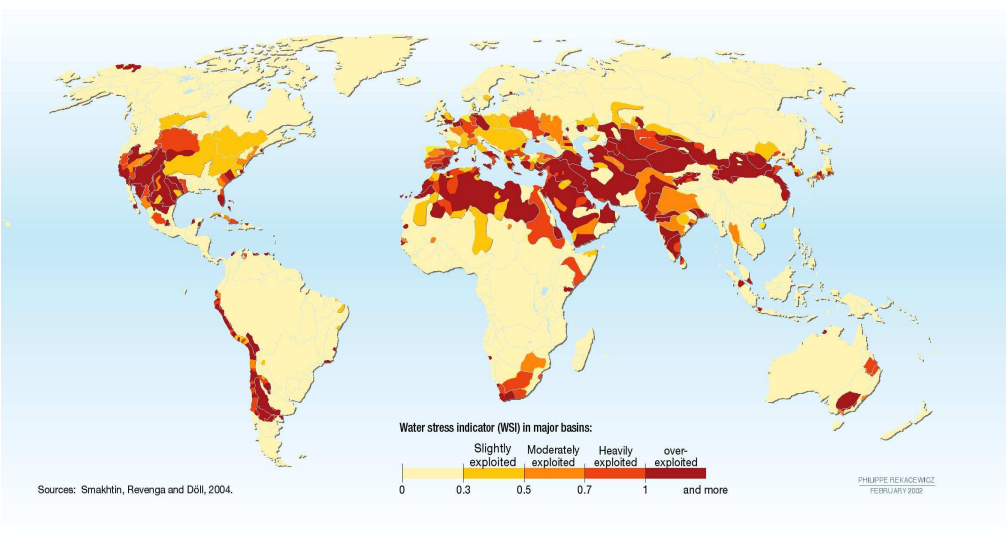

Figure 3.2 Water Stress Indicator in major basins
(source: http://www.unep.org/dewa/vitalwater/article77.html)

The result of the sensitivity analysis are summarized in Table 3.1. Result shows that for the 11 river sections in the four U.S. rivers used for comparison. And Figure 3.3 gives the location of gauging stations along these rivers. Slope calculated using 20 km river segments yielded the largest difference from the observed slope. The 50 km and 100 km results were very similar in most river segments. The 50 km splitting product performs the best and the 20 km is the worst. The 50 km and 100 km result performs better than the 20 km likely because of the resolution of the DEM used in this study. The results of the 50 km threshold is a slightly better than 100 km likely due to an increase in the resulting slope layer resolution. The 50 km threshold was therefore used for the global scale calculation and 6 arc-min upscaling.

Table 3.1 Summery of the calculated and estimated river slope along four U.S. rivers (measured values are from Calston CW, 1969; Biedenharn et al., 1999)

Rivers	Gauge Stations	Average slope calculated from different length of river segments (m/m)						Measured Slope (m/m)
		20000m		50000m		100000m		
		Slope Value	% Diff	Slope Value	% Diff	Slope Value	% Diff	Slope Value
Mississippi River	New Madrid to Fulton	0.00042	366%	0.00031	237%	0.00036	297%	0.00009
	Fulton to Sunflower	0.00066	590%	0.00045	375%	0.00045	370%	0.00010
	Sunflower to Rosedale	0.00058	590%	0.00028	239%	0.00023	173%	0.00008
	Rosedale to Lake Providence	0.00062	712%	0.00035	361%	0.00029	282%	0.00008
	Lake Providence to Vicksburg	0.00043	560%	0.00028	329%	0.00024	268%	0.00007
	Vicksburg to Nathez	0.00056	857%	0.00039	574%	0.00053	816%	0.00006
Roanoke River	Entire river	0.00181	166%	0.00146	114%	0.00159	134%	0.00068
Arkansas River	Salt Fork River to Verdigris River	0.00088	103%	0.00058	34%	0.00057	32%	0.00043
	Poteau River to Bayou Meto	0.00084	547%	0.00071	448%	0.00071	449%	0.00013
Ohio River	Cairo IL to Louisville	0.00117	1984%	0.00091	1530%	0.00090	1507%	0.00006
	Louisville to Pittsburgh	0.00226	2443%	0.00206	2218%	0.00196	2104%	0.00009
Average Slope of Four American Rivers		0.00093	451%	0.00071	320%	0.00071	323%	0.00017
RMSE value		0.00092		0.00023		0.00024		

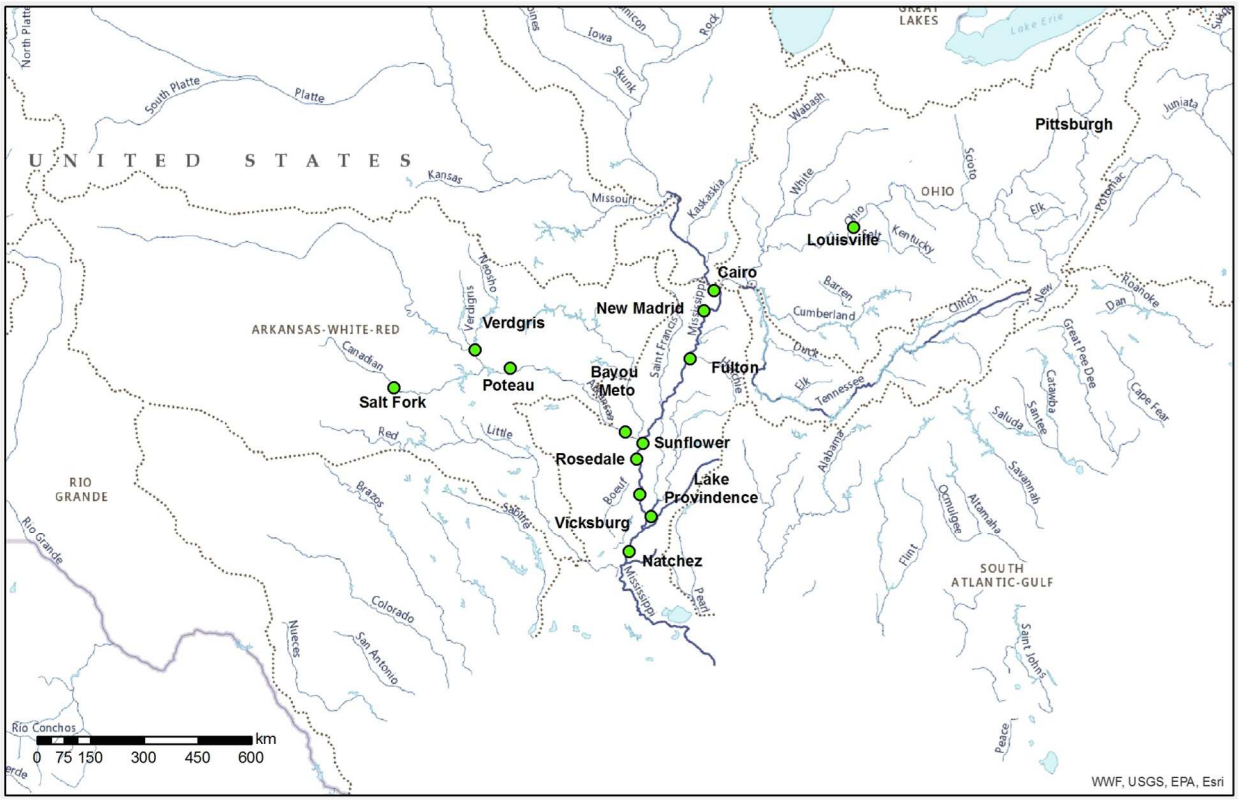

Figure 3.3 Location of river reaches with estimated slope values based on *Calston CW, 1969; Biedenharn et al., 1999.* Green dots show the distribution of gauges, blue line shows large American rivers, while brown dotted lines are boundaries of water basins. Measured slopes in Table 3.1 are observed river's slopes between each gauge stations.

The slope 6 arc-min upscaled slope layer (based on the 50 km splitting threshold) was evaluated against the NH plus dataset. Five hundred random points were generated along rivers with a total drainage area larger than 1000 km^2 (approximately 10x10 6 arc-min grid-cells). The slope values from the 6 arc-min and NHDplus layers were extracted for these 500 points. To reduce biases in this comparison due to differences in the location of the river networks in the two layers, the recorded contributing area were also compared. Points in which the difference between the two layers' contributing areas was +/- 15% were removed from the analysis. The NHDplus dataset also include many stream features with a calculated slope of zero. Points that fell on these reaches were also removed from the analysis. The result of the slope comparison for the remaining 173 points between two datasets is shown in Figure 3.4.

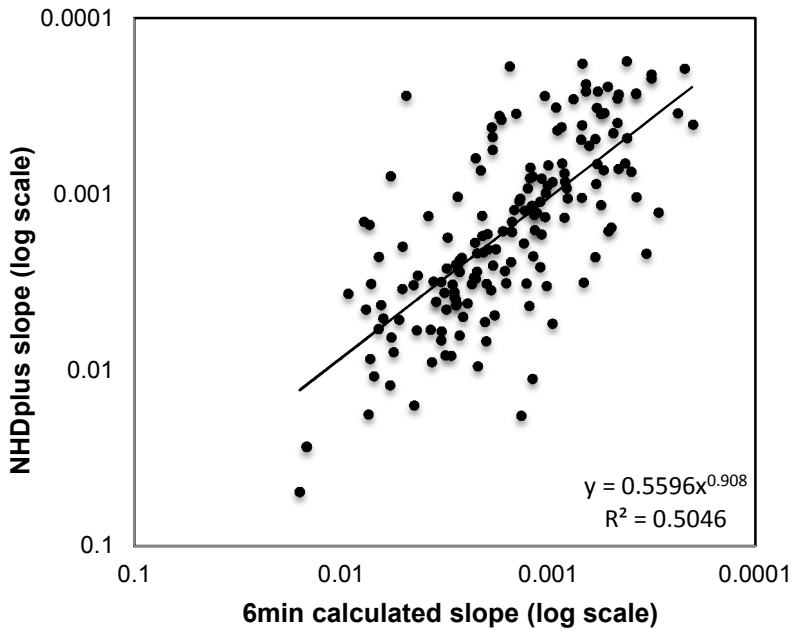

Figure 3.4 Comparison between the 6 arc-min and NHDplus slope values in 173 random points along U.S. rivers with drainage areas over 1000 km^2

The correspondence between the two layers is not strong ($R^2 = 0.5$). It has a good, close to 1:1, trend but with considerable scatter. This is however a fairly promising result considering

the very low slopes values relative to the spatial resolution of the slope layer (average of about 0.001m/m and over 100 km^2 respectively). Also, NHDplus is in itself a calculated dataset and therefore prone to its own biases. And this can also be obtained from the average slope for these 173 points. The average for 6 min raster is 0.0023 while the average for NHDplus is 0.003. Generally, for each point along rivers, the slope simulated by NHDplus is slightly greater than the value we calculated.

Figure 3.5 show the percent difference between the two datasets in the 173 random points as a function of contributing area. While there is a distinct decrease in the number of high percent difference values with increasing contributing area the overall trend is not significant (R^2< 0.001). It can therefore be concluded that predictions in larger rivers is likely somewhat more robust but the methodology accuracy is not strongly dependent on contributing area at these ranges (> 1000 km^2).

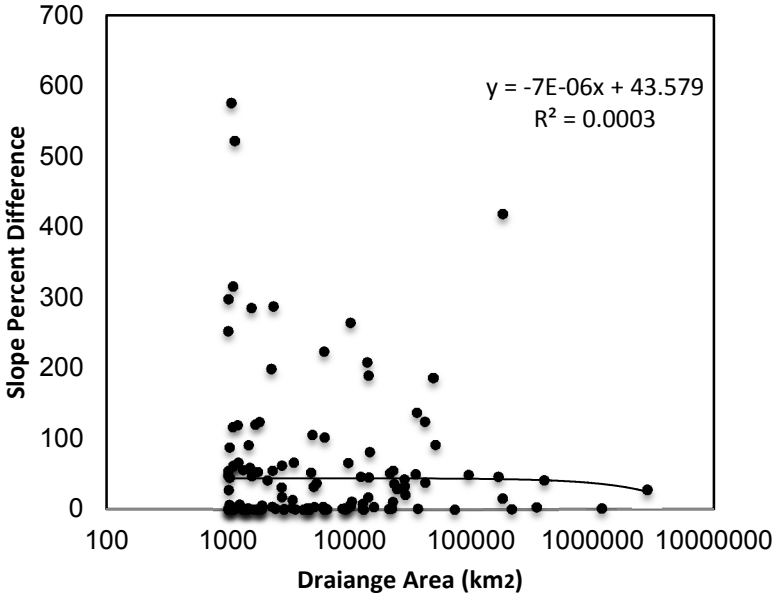

Figure 3.5 Difference slope and drainage area

The 6 arc-min and the NHDplus slope values were compared to reported (from the literature) slope estimates in 11 rivers (Table 3.2). These slope observations are also based on

calculation of elevation depression along long-river reaches (between USGS gauging stations; ranging from 68 to 982 km). NHDplus slope values for each of these river reaches were extracted by averaging all the NHDplus river segments along the reaches. The 6 arc-min slope values were extracted by averaging the grid-cells along these 11 river reaches. Most of these river reaches are around 100 – 200km in length, which is most appropriate for this comparison. The Ohio River is an exception in which the lengths of river sections are significantly longer than the other rivers used in this analysis (Table 3.2). Every Ohio River section contains more than 20 river segments, which leads to a big difference between observed slope and simulated slope, likely due to miss match in the stream networks' overlap. Two comparisons were therefore preformed, one that includes the Ohio River and the other that does not (Figure 3.6 and 3.7).

Table 3.2 Simulated and Observed Slope Values for 4 US Rivers

River	Range	Length (km)	River Slope		
			6min_ras (m/m)	Observed (m/m)	NHDplus (m/m)
Arkansas River	Salt Fork River to Verdigris River	286	0.000655	0.000430	0.001001
Arkansas River	Poteau River to Bay Meto	499	0.000519	0.000130	0.000441
Roanoke River		659	0.000837	0.000680	0.001830
Mississippi River	New Madrid to Fulton	177.2	0.000332	0.000091	0.000082
Mississippi River	Fulton to Sunflower	281.7	0.000292	0.000095	0.000140
Mississippi River	Sunflower to Rosedale	68	0.000383	0.000083	0.000114
Mississippi River	Rosedale to Lake Providence	197	0.000283	0.000076	0.000040
Mississippi River	Lake Providence to Vicksburg	90.5	0.000250	0.000065	0.000115
Mississippi River	Vicksburg to Natchez	145.7	0.000329	0.000058	0.000154
Ohio River	Cairo IL to Louisville	595	0.000696	0.000056	0.000067
Ohio River	Louisville to Pittsburgh	982	0.000954	0.000089	0.000011

(Length represents the length of the corresponding river section, 6min_ras provides slope values we calculated, NHDplus gives slope values simulated by NHDplus and Observed values are values gained from field measurements summarized from literatures)

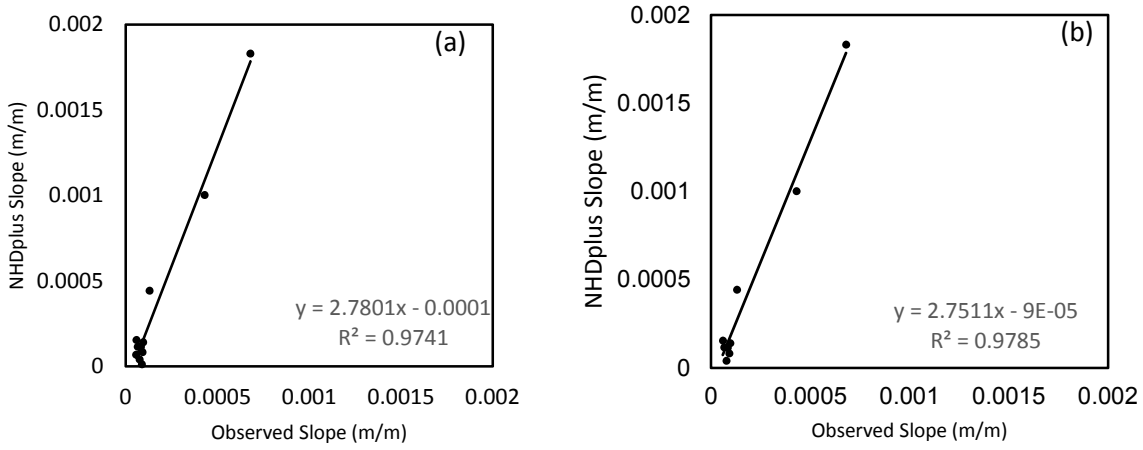

Figure 3.6 Comparisons between NHDplus Slope and Observed Slope for US Rivers; (a) including the Ohio River and (b) not including the Ohio River

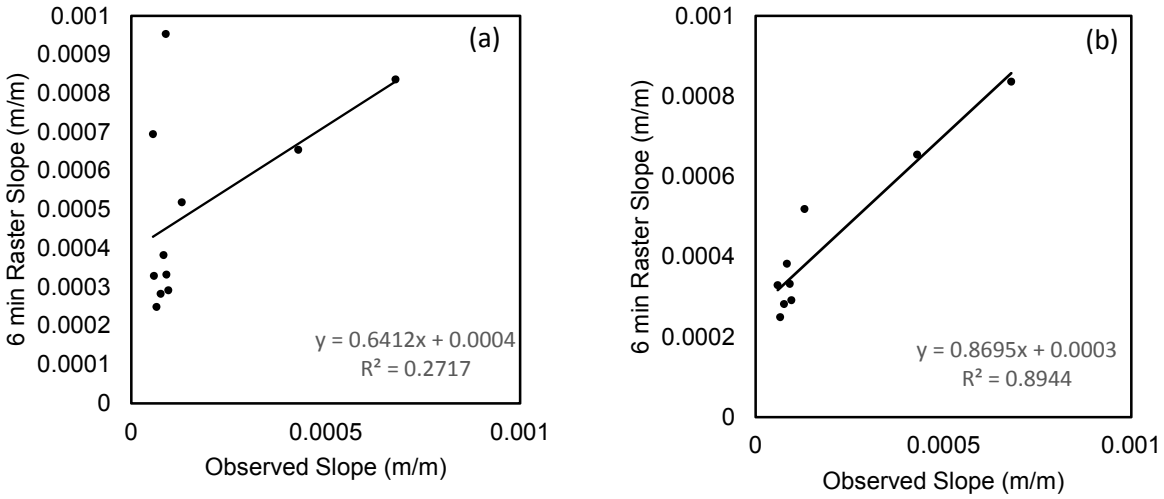

Figure 3.7 Comparisons between 6 min Raster Slope and Observed Slope for US Rivers; (a) including the Ohio River and (b) not including the Ohio River

Figure 3.6a and 3.6b show that NHDplus slope values strongly corresponds to variations in observed slope values but with considerable overestimation. Based on the strong correlation

between NHDplus and observed slopes, it can be considered as a good representative of spatial trends in river's slope.

Figure 3.7a and b show the relationship between calculated 6 arc-min raster slope and observations. It can be seen that Fig. 3.7a has a higher R^2 than Fig. 3.7b, which indicates that without the Ohio River, the method simulates actual slope very accurate with an R^2 close to 0.9. The 6 arc-min layer also overestimate slope values but not as much as the NHDplus dataset. The difference accuracy introduced by the Ohio River can be explained by its large amount of segments along this longer the river section. More segments are more likely to lead to less accurate comparison due to miss match between the river networks. The Ohio River is also a very shallow river with a low slope (Table 3.2).

Since we used the 15 sec DEM data to calculate the slope, we can hardly generate a very low slope such as the Ohio River's, especially for large and long rivers.

RMSE (Root Mean Square Error) was calculated to show the slope difference between simulated slope and observed slope. Table 3.3 shows the average slope for the 6 arc-min raster and NHDplus in the 11 river reaches and the RMSE of both 6 arc-min raster slope and NHDplus slope against observed slope values. NHDplus and the 6 arc-min raster average slope and RMSE are overall very similar. The 6 arc-min raster RMSE is slightly smaller reflecting to the aforedescribed lower overestimation bias. Figure 3.6 and 3.7 show that NHDplus simulates actual slope better than 6 arc-min raster slope based on the R2. But the bias is very large between NHDplus and observations. This may because Figure 3.6 compare NHDplus slope with observed slope based on river sections, not specific points. The slope values of the NHDplus segments have many 0.000 and 0.00001 (a flat minimum value in the dataset) slope values. The relatively large number of segments with low values can significantly lower the average slope calculated

for the NHDplus. This may explain the stronger correspondence of the NHDplus values in the Ohio river for example and indicate that the actual overestimation of this dataset are realistically higher than shown in this analysis. This also show that the NHDplus dataset is less spatially resolved than the 6 arc-min as it contain many 0.000 and 0.00001 slope values.

Table 3.3 RMSE for simulated slope values and observed slope values

	6 arc-min Raster Slope	NHDplus Slope
Average Slope	0.0005	0.0004
RMSE	0.0003	0.0004

Five additional observed river slopes values along global rivers (three river sections in the Amazon River and two sections of the Yangtze River) were used to validate the 6 arc-min slope result (Table 3.4 below). The NHDplus dataset was not incorporated in this analysis as it only covers U.S. rivers. The calculated 6 arc-min raster overestimate the observed slope for the selected river sections. The correlation between observed and calculated slope is very strong but with very high trend slope (Figure 3.8a). Given that the bias in 6 arc-min predictions is consistent across the range of observed values, an adjustment factor can be used to improve the calculated slope values. Since the bias shows that calculated values are generally 8 times greater than observed values, the slope values were divided by 8 for all 5 points (Figure 3.8b). Further analysis is needed to determine whether this adjustment factor should be applied globally.

Table 3.4 calculated 6 min raster slope and observed slope for the Amazon River and the Yangtze River

River	**Range**	**River Slope** (m/m)	
		Observed	6 arc-min
Amazon River	Iquitos to Santo Antonio do Ica	0.00006	0.000701
Amazon River	Santo Antonio do Ica to Itapúa	0.00004	0.000519
Amazon River	Itapúa to Manacapuru	0.00002	0.000398
Yangtze River	Hankou-Poyang lake	0.000025	0.000355
Yangtze River	Poyang lake-Wuhu	0.000015	0.000294
Average		0.000032	0.00045

(Data Resources: R.H. Meade et al., 1991; Stroebe, G.G., 1925)

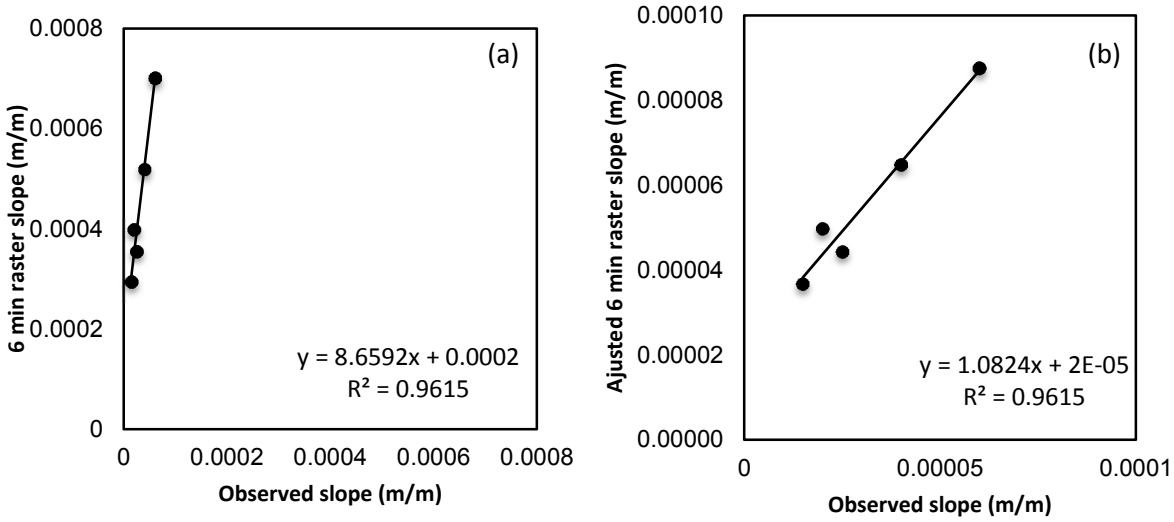

Figure 3.8 Calculated 6 min raster slope and Observed slope for the Amazon River and the Yangtze River; (a) before being adjusted and (b) after being adjusted

CHAPTER 4

FURTHER APPLICATIONS

Overall the 6 arc-min global river's slope data is significantly similar to result from NHDplus and to some extent better fits observations. This dataset can be used in both hydrological and geomorphic models, which deal with fluvial processes on large rivers. Some specific application of this dataset is using this slope data to determine the bedload flux at a global scale.

Bedload is a significant part of the fluvial sediment budget and its transport is an inherent physical process in alluvial channel (Gomez, 1991). Many researches have been conducted on fluvial bedload have focused on small rivers or investigate scale due to the difficult of accurately and continuously measuring bedload flux in large rivers (Milliman & Farnsworth, 2011). Attempts to understand bedload transport from developing a bedload equation and simulating bedload transport show that slope is a key variable (e.g. Meyer Peter and Muller, 1948; Bagnold, 1980; Parker, 1990). Frequently used equations such as the MPM equation, Parker's equation and Bagnold's equation all set river's slope as a factor in this bedload function. One of the challenges in applying these equations in large-scale modeling frameworks is realistic representation of river's slope. The new global river's slope dataset presented here provides the possibility for us to simulate bedload flux at a larger scale.

WBMsed model is the first spatially-explicit global river's sediment flux model (Cohen et al., 2013a, 2014) and is able to provide a complete and useful modeling framework to generate

a bedload module that simulates bedload flux based on bedload equations in since it already simulates most of the hydrological and morphological variables of these equations (e.g. discharge, velocity, slope and width). The global slope layer presented here is currently used to incorporate the modified Bagnold (1966) equation into the WBMsed framework. The simplified Bagnold (1966) equation is:

$$Q_b = Q_i S \frac{\rho_s \rho e_b}{(\rho_s - \rho) tan\lambda} \quad (3)$$

where Q_b is daily bedload flux (kg/s), S is delta plain slope (m/m), Qi is daily mean water discharge (m^3/s), ρ_s is sediment density (kg/m^3), ρ is fluid density (kg/m^3), e_b is the bedload efficiency, λ is the limiting angle of repose of sediment grains lying on the river bed. Since this equation will be applied under WBMsed framework, Qi will be automatically simulated by WBMsed model temporal and spatial dynamic. Slope will be obtained from the 6 arc-min raster slope layer. All other parameters can be set up as constant values. Once this model is fully developed and tested it will provide the spatially and temporally explicit global bedload flux estimations.

CHAPTER 5

CONCLUSIONS

Generating a new global river's slope dataset is attractive for improving the comprehension of a large amount of fluvial processes and patterns. Since slope plays such an important role in a variety of geomorphological and hydrological regimes, an accurate slope data can help determine characteristics of rivers and river dynamics. A methodology for calculating large scale river's slope based was presented. The resulting dataset can fill the gap of observational deficiency in the vast majority of global rivers and realize the goal of calculating slope globally instead of for each location.

The methodology presented here has been validated against observations and other calculated results (NHDplus dataset for U.S. rivers). The validation results show that the calculated slope corresponds relatively well to both NHDplus and observed slope values. For some large river sections, particularly with a very low slope values, the validation result shows that calculated slope overestimates observed slope at a factor of 5-8. This bias is likely due to a combination of two aspects. One is that the 6 arc-min raster slope was calculated from a relatively coarse resolution DEM which cannot capture the elevation depression information accurately enough in very low slope river reaches. Second, for long river sections, the validation method is not accurate enough. Using the average slope value to represent a river contains a large amount of river segments causes the bias to observed slope. This problem could be solved by collecting more observed slope data for a short river section or a specific point along rivers and then compare these observations with the simulated slope data.

Generally, this method generated a global river's slope raster with a resolution of 6 arc-min. This slope dataset has been validated that it generally simulates the world's rivers slope accurate enough to be further used. Furthermore, this dataset can be applied with upscaling to coarser resolutions that meet requirements of other hydrological models. It addresses a key knowledge and predictive capabilities of variables in large river are still lacking. A global slope dataset can also be helpful in studying river evolution and dynamics.

REFERENCES

Arora, V. K., & Boer, G. J. (1999). A variable velocity flow routing algorithm for GCMs. *Journal of Geophysical Research: Atmospheres*, 104(D24), 30965-30979.

Bagnold, R. A. (1966). An approach to the sediment transport problem. *General Physics Geological Survey*, Prof. paper.

Bagnold, R. A. (1980, October). An empirical correlation of bedload transport rates in flumes and natural rivers. In Proceedings of the Royal Society of London A: *Mathematical, Physical and Engineering Sciences* (Vol. 372, No. 1751, pp. 453-473). The Royal Society.

Biedenharn, D. S., Thorne, C. R., & Watson, C. C. (2000). Recent morphological evolution of the Lower Mississippi River. *Geomorphology*, 34(3), 227-249.

Bridge, J. S. (2003). Rivers and Floodplains, 491 pp.

Burrough, P. A. (1996). Natural objects with indeterminate boundaries. *Geographic objects with indeterminate boundaries*, 2, 3-28.

Burbank, D. W., & Anderson, R. S. (2011). *Tectonic geomorphology*. John Wiley & Sons.

Carlston, C. W. (1969). Longitudinal slope characteristics of rivers of the midcontinent and the Atlantic East Gulf Slopes. *International Association of Scientific Hydrology*. Bulletin, 14(4), 21-31.

Cohen, S., Kettner, A. J., Syvitski, J. P., & Fekete, B. M. (2013). WBMsed, a distributed global-scale river's sediment flux model: Model description and validation. *Computers & Geosciences*, 53, 80-93.

Cohen, S., Kettner, A. J., & Syvitski, J. P. (2014). Global suspended sediment and water discharge dynamics between 1960 and 2010: Continental trends and intra-basin sensitivity. *global and planetary change*, 115, 44-58.

Du Boys, M. P. (1879). The Rhone and streams with movable beds. *Annals des Pontes et Chaussees*, 18, 22.

Fekete, B. M., Vörösmarty, C. J., & Lammers, R. B. (2001). Scaling gridded river networks for macroscale hydrology: Development, analysis, and control of error. *Water Resources Research*, 37(7), 1955-1967.

Gilbert, G. K. (1877). *Report on the Geology of the Henry Mountains*. US Government Printing Office.

Gomez, B. (1991). Bedload transport. *Earth-Science Reviews*, 31(2), 89-132.

Gregory, D. I., & Schumm, S. A. (1987). The effect of active tectonics on alluvial river morphology. Richards,(Ed.) *River Channels: Environment and Process. Blackwell, Oxford*, 41-68.

Hagemann, S., & Dümenil, L. (1997). A parametrization of the lateral waterflow for the global scale. *Climate Dynamics*, 14(1), 17-31.

Hannon, M. T. (2011). Exploring Predictive Relationships of Fluvial Morphology: Using Shuttle Radar Topography Mission Data. M.Sc. Thesis, University of Colorado Boulder.

Holbrook, J., & Schumm, S. A. (1999). Geomorphic and sedimentary response of rivers to tectonic deformation: a brief review and critique of a tool for recognizing subtle epeirogenic deformation in modern and ancient settings. *Tectonophysics*, 305(1), 287-306.

Kettner, A. J., & Syvitski, J. P. (2008). HydroTrend v. 3.0: A climate-driven hydrological transport model that simulates discharge and sediment load leaving a river system. *Computers & Geosciences*, 34(10), 1170-1183.

Knighton, A. D. (1999). Downstream variation in stream power. *Geomorphology*, 29(3), 293-306.

Lin, W. T., Chou, W. C., Lin, C. Y., Huang, P. H., & Tsai, J. S. (2006). Automated suitable drainage network extraction from digital elevation models in Taiwan's upstream watersheds. *Hydrological Processes*, 20(2), 289-306.

Manning, R., Griffith, J. P., Pigot, T. F., & Vernon-Harcourt, L. F. (1890). On the flow of water in open channels and pipes.

Mackin, J. H. (1948). Concept of the graded river. *Geological Society of America Bulletin*, 59(5), 463-512.

Mayorga, E., Logsdon, M. G., Ballester, M. V. R., & Richey, J. E. (2005). Estimating cell-to-cell land surface drainage paths from digital channel networks, with an application to the Amazon basin. *Journal of Hydrology*, 315(1), 167-182.

McKay L, Bondelid T, Rea A, Johnston C, Moore R, Dewald T (2012) NHDPlus Version 2: User Guide. Available at: http://www.horizon-systems.com/nhdplus/ NHDPlusV2_documentation.php (accessed 27 March 2012).

Meyer-Peter, E., & Müller, R. (1948, June). Formulas for bed-load transport. IAHR.

Milliman, J. D., & Farnsworth, K. L. (2011). Runoff, erosion, and delivery to the coastal ocean. *River discharge to the coastal ocean: a global synthesis, Cambridge University Press, Cambridge, UK*, 13-69.

Montgomery, D. R., & Brandon, M. T. (2002). Topographic controls on erosion rates in tectonically active mountain ranges. *Earth and Planetary Science Letters*, 201(3), 481-489.

Moore, I. D., Grayson, R. B., & Ladson, A. R. (1991). Digital terrain modelling: a review of hydrological, geomorphological, and biological applications. *Hydrological processes*, 5(1), 3-30.

Ngo-Duc, T., Oki, T., & Kanae, S. (2007). A variable streamflow velocity method for global river routing model: model description and preliminary results. *Hydrology and Earth System Sciences Discussions*, 4(6), 4389-4414.

O'Callaghan, J. F., & Mark, D. M. (1984). The extraction of drainage networks from digital elevation data. *Computer vision, graphics, and image processing*, 28(3), 323-344.

Olivera, F. (2001). Extracting hydrologic information from spatial data for HMS modeling. *Journal of Hydrologic Engineering*, 6(6), 524-530.

Olivera, F., & Raina, R. (2003). DEVELOPMENT OF LARGE SCALE GRIDDED RIVER NETWORKS FROM VECTOR STREAM DATA1.

Parker, G. (1990). Surface-based bedload transport relation for gravel rivers. *Journal of hydraulic research*, 28(4), 417-436.

Reed, S. M. (2003). Deriving flow directions for coarse□resolution (1–4 km) gridded hydrologic modeling. *Water resources research*, 39(9).

R.H. Meade et al., 1991 Backwater effects in the Amazon River basin of Brazil. Environmental *Geology and Water Sciences*, 18(2), 105-114.

Schulze, K., Hunger, M., & Döll, P. (2005). Simulating river flow velocity on global scale. *Advances in Geosciences*, 5, 133-136.

Schumm, S. A. (1986). Alluvial river response to active tectonics. *Active tectonics*, 80-94.

Schumm, S. A., Dumont, J. F., & Holbrook, J. M. (2000). *Active Tectonics and Alluvial Rivers* Cambridge University Press.

Snow, R. S., & Slingerland, R. L. (1987). Mathematical modeling of graded river profiles. *The Journal of Geology*, 15-33.

Stroebe, G.G., 1925 Some hydrological facts concerning the Yangtze: *Association of Chinese and American Engineers Journal*, v.6, p.22-31, pl. 1-25)

Strahler, A. N. (1957). Quantitative analysis of watershed geomorphology. *Eos, Transactions American Geophysical Union*, 38(6), 913-920.

Thieken, A. H., LuÈcke, A., DiekkruÈger, B., & Richter, O. (1999). Scaling input data by GIS for hydrological modelling. *Hydrological processes*, 13(4), 611-630.

Verzano, K., Bärlund, I., Flörke, M., Lehner, B., Kynast, E., Voß, F., & Alcamo, J. (2012). Modeling variable river flow velocity on continental scale: Current situation and climate change impacts in Europe. *Journal of Hydrology*, 424, 238-251.

Walker, J. P., & Willgoose, G. R. (1999). On the effect of digital elevation model accuracy on hydrology and geomorphology. *Water Resources Research*, 35(7), 2259-2268.

Data Resources:

Hydrosheds: http://hydrosheds.cr.usgs.gov/index.php

ETOPO1 1 Arc-Minute Global Relief Model: Procedures, Data Sources and Analysis. NOAA Technical Memorandum NESDIS NGDC-24. National Geophysical Data Center, NOAA. doi:10.7289/V5C8276M

NHDplus V2: Available: www. horizon-systems. com/NHDPlus/index. php.(October 2014).